Chinese Journal of Aeronautics, (2014),27(5): 1097–1110

Chinese Society of Aeronautics and Astronautics
& Beihang University

Chinese Journal of Aeronautics

cja@buaa.edu.cn
www.sciencedirect.com

Design for aircraft engine multi-objective controllers with switching characteristics

Liu Xiaofeng [a,*], Shi Jing [a], Qi Yiwen [b], Yuan Ye [c]

[a] School of Transportation Science and Engineering, Beihang University, Beijing 100191, China
[b] School of Automation, Shenyang Aerospace University, Shenyang 110136, China
[c] School of Energy and Power Engineering, Beihang University, Beijing 100191, China

Received 24 July 2013; revised 14 April 2014; accepted 7 May 2014
Available online 20 August 2014

KEYWORDS

Aircraft engine;
Compensatory controller;
Min/Max switching;
Multi-objectives control;
Smooth switching;
Switching scheme

Abstract The aircraft engine multi-loop control system is described and the switching control theory is introduced to solve the regulating and protecting control problems in this paper. The aircraft engine multi-loop control system is firstly described and the control problems are formulated. Secondly, the theory of the smooth switching control is devoted and a new extended scheme for the smooth switching of a switched control system is introduced. Then, for the key technologies of aero-engines switching control, a design algorithm is presented which can determine which candidate controller should be put in feedback with the plant to achieve a desired performance and the procedure to design the aircraft engine multi-loop control system is detailed. The switching performance objectives and the switching scheme are given and a family of PID controllers and compensators is designed. The simulation shows that using the switching control design method can not only improve the dynamic performance of the aircraft engine control system and reduce the switching times, but also guarantee the stability in some peculiar occasions.

1. Introduction

With the development of advanced aircraft engine technology, the control technology plays an increasingly important role. Because the aircraft engines have become more complex, with more control signals and higher demands on performance and functionality, electronic control systems have been introduced.[1,2] The experience of development of the aircraft engines in the world shows that the performance parameters of aircraft engines, such as thrust, specific fuel consumption, surge margin, etc., can be changed to a certain extent in order to increase aircraft engines function, adaptation and reliability to meet the requirements of different potential users and can be implemented only by using advanced control modes and control laws, causing little change on the aircraft engines' hardware.

The aircraft engine is a complex nonlinear system operated in an uncertain environment of limits: limits in temperature, air pressure and physical acceleration, etc. Aircraft engine

* Corresponding author. Tel.: +86 10 82316627.
E-mail addresses: liuxf@buaa.edu.cn (X. Liu), zhongai619@sina.com (J. Shi), qiyiwen@gmail.com (Y. Qi), desertdeagle@163.com (Y. Yuan).

Peer review under responsibility of Editorial Committee of CJA.

Production and hosting by Elsevier

http://dx.doi.org/10.1016/j.cja.2014.08.002

control systems can be designed by using linearized engine models under the multiple trimmed flight conditions throughout the flight envelope. For each of these operating points a corresponding linear controller is derived using the well-established linear-based control design methods.[3–5] However, a problem of this approach is that good performance and robustness properties cannot be guaranteed for a highly nonlinear aircraft engine. Nonlinear control methods have been developed to overcome the shortcomings of linear design approaches.

Several nonlinear control system design methods have emerged over the past two decades.[6–9] The theoretically established feedback linearization approach is the best known and most widely used among these methods. Feedback linearization is a nonlinear design method that can explicitly handle systems with known nonlinearities. By using nonlinear feedback and exact state transformations rather than linear approximations the nonlinear system is transformed into a constant linear system. This linear system can in principle be controlled by just a single linear controller.[10,11]

During the past decade, switched systems have attracted significant attention, because they can model several practical control problems that involve the integration of supervisory logic-based control schemes and feedback control algorithms. And the results have been developed for linear[12] and nonlinear systems.[13–15] Concerning output feedback control of switched systems, the results are as follows. In Ref.[16], by checking the existence of a switched Lyapunov function, linear matrix inequality-based sufficient conditions are derived to deal with the switched static output feedback control of discrete-time switched systems under arbitrary switching. Since there exist linear time-invariant systems, which cannot be stabilized via a single static output feedback, research has been dedicated to the study of hybrid static output feedback stabilization of linear time-invariant systems.[17–21] In Ref.[22], the output feedback robust stabilizability problem for uncertain dynamic systems is also considered.

The outline of this paper is as follows. First, the aircraft engine multi-loop control system is described in Section 2 and the control problems are formulated. Section 3 is devoted to the theory of the smooth switching control; a new extended scheme for the smooth switching of a switched control system and an algorithm is also presented in this section. Section 4 shows the procedure to design the aircraft engine multi-loop control system and the simulation results and comparisons. Finally, the conclusion can be obtained in Section 5.

2. Description of aircraft engine multi-loop control system

2.1. Aircraft engine descriptions

No matter for the linear or nonlinear control system design methods, the aircraft engine will encounter limits on some occasions. So the aircraft engine control system consists of a family of continuous-time subsystems and switches from one to another depending on various environmental factors (see Fig. 1). When the aircraft engine switches from one sub-control loop to another, the stability of the system is the basic performance that must be considered. Therefore, there is much space to improve the dynamic performance of the control system.

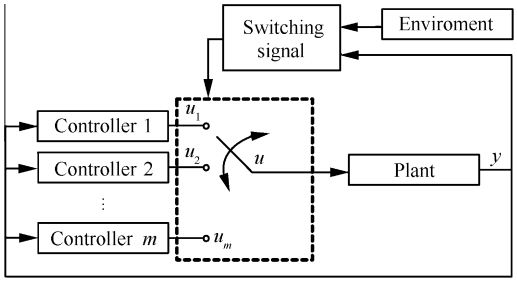

Fig. 1 Architecture of multi-controllers.

In this section, the aircraft engine of two-spool turbofan engine model was developed by the MATLAB simulation environment and its Simulink toolbox. The schematic configuration of the turbofan engine that was simulated is shown in Fig. 2. The high pressure compressor (HPC) and high pressure turbine (HPT) are on one shaft (driven by the high speed rotor), while the fan, booster and low pressure turbine (LPT) are on the other shaft (driven by the low speed rotor). Bleed effects (for air bleed from the booster and the compressor) are not currently considered in the model.

The engine simulation model, which is called nonlinear component level (NCL) model, consists of the static elements: inlet, fan (single stage), booster (four stages), high pressure compressor (nine stages), combustor, high pressure turbine (single stage), low pressure turbine (four stages) and main nozzle which are modeled as lumped parameter thermodynamic systems, represented by performance maps, constant coefficients, and thermo and aero-dynamic relationships and the dynamic elements which include low speed rotor and high speed rotor. In the model, the rotor dynamics (for the high speed and low speed rotors) is represented by the equation of conservation of angular momentum. Components, including the fan, the compressor and the turbines, are described in the form of maps and look-up tables based on their individual experimental data. The combustion efficiency and pressure losses are simply fitted by curves. Fig. 3 shows the characteristics of the turbofan engine typical components. In Fig. 3, π_F, η_F, $w_{a,cor,F}$ are fan pressure ratio, fan efficiency, and fan corrected air mass flow; π_B, η_B, $w_{a,cor,B}$ are booster pressure ratio, booster efficiency, and booster corrected air mass flow; π_C, η_C, $w_{a,cor,C}$ are compressor pressure ratio, compressor efficiency, and compressor corrected air mass flow.

2.2. Multi-objective with aircraft engine

As a modern aircraft, in order to achieve high performance flights, a high performance aircraft engine control system is essentially indispensable. But there are also many limits during the aircraft engine working process. For example, when the aircraft engine accelerates from one stable condition to another, the compressor surge imposes limits on the aircraft engine operation.

Fig. 4 shows the limit represented by the surge line. The surge line demarcates the regions between stable and unstable operation of the compressor. If the accelerating line goes through the surge line, the stability of the aircraft engine working condition is destroyed. Therefore, the aircraft engine

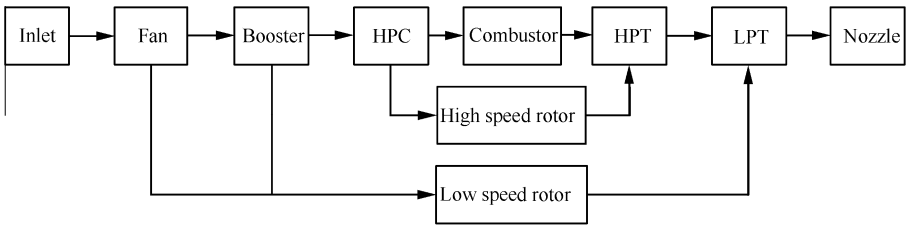

Fig. 2 Schematic configuration of two-spool turbofan engine.

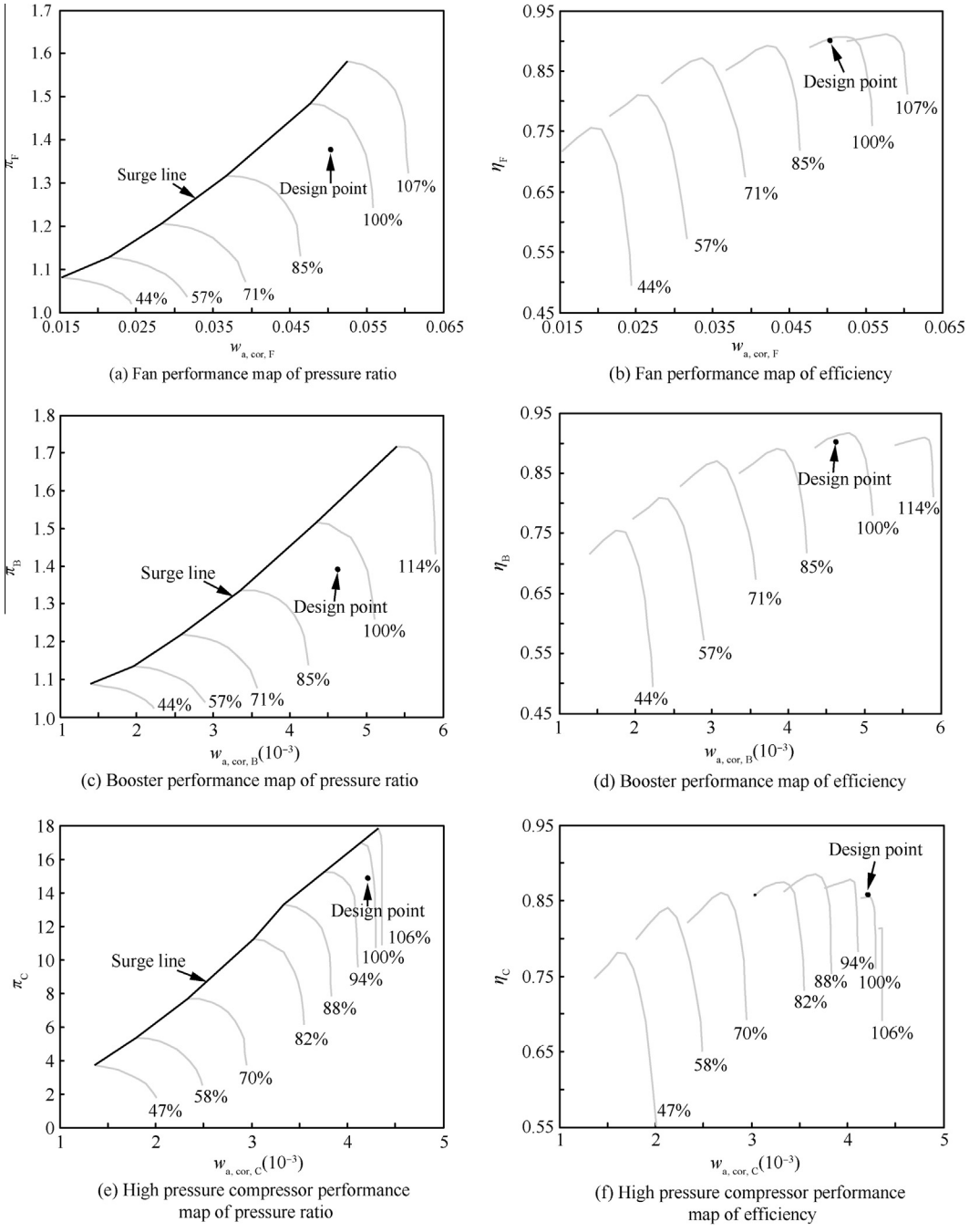

Fig. 3 Characteristics of turbofan engine typical components.

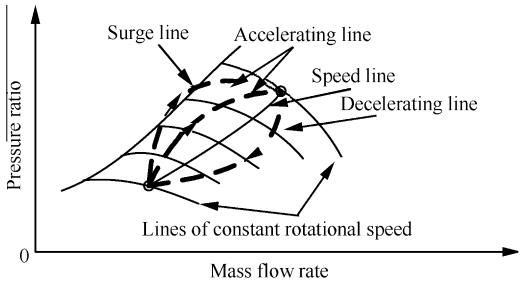

Fig. 4 Maps of aircraft engine working characteristics.

control system has to switch to a stable control loop to avoid the unstable surge oscillation.

Also in the accelerating process, the more fuel flow can cause the excess air coefficient to go through the rich blow-out line (see Fig. 5), resulting in a combustor blow-out event and loss of thrust. So the aircraft engine control system has to switch from the accelerating control loop to another stable control loop, such as speed control loop.

If a limit of turbine temperature is encountered, the remaining command has no effect on an engine. The condition is known as dead-stick and is said to be rather disconcerting. Fig. 6 shows the phenomenon. The pilot lever generates a speed governing and a temperature governing characteristic (Curves 1 and 2, respectively). As speed increases along Curve 1, turbine temperature may rise according to Curve 3. If the temperature reaches its permissible limit before the speed attains its maximum value, Curve 3 must intersect Curve 2. This condition can be detected by equality of the two voltage signals representing a demand and an observed temperature. Control can be smoothly transferred from Curve 1 to Curve 2 over the remaining portion of lever movement, and conversely, as the lever is returned to a lower speed demand. The principle is obviously applicable to several protection controls; whichever parameter reaches its control line first determines the final mode of control. Therefore, the safe working regions are shown in Fig. 7.

2.3. Regulation and protection of multi-loops controllers

As for the rotary speed control of twin shafts engines, one shaft is already controllable, the other one can be controlled by aerodynamic match. Both spools need to be independently protected against over-speed conditions. Fig. 8 illustrates a typical complex control requirement. The speed of the high pressure spool is controlled by the pilot lever angle. To achieve

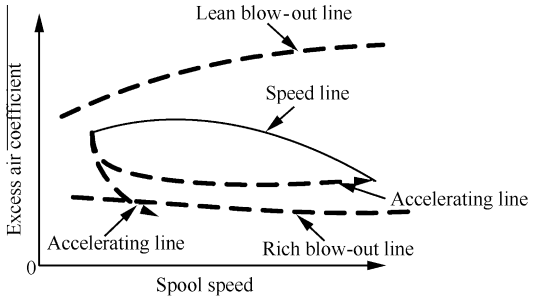

Fig. 5 Variation of excess air coefficient with spool speed.

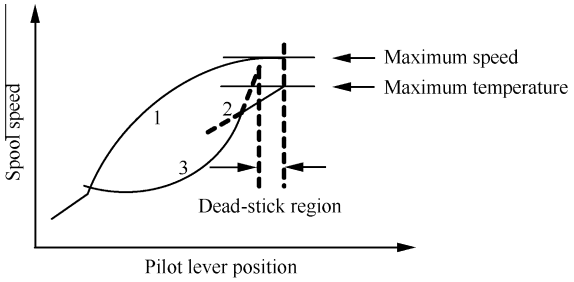

Fig. 6 Illustration of dead-stick conditions and possible method for avoidance.

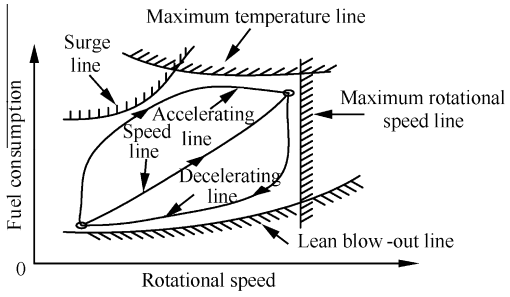

Fig. 7 Limits of the aircraft engine works.

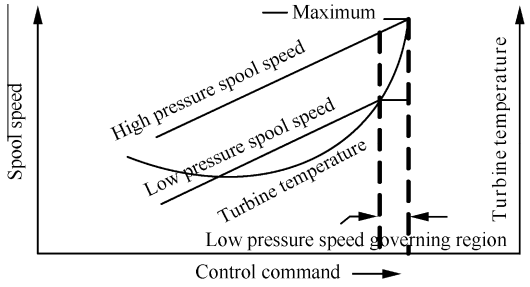

Fig. 8 Ilustration of typical engine control requirements.

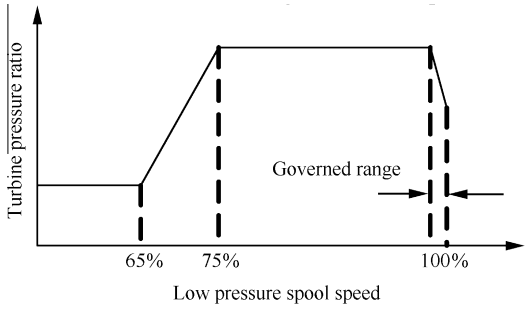

Fig. 9 Turbine pressure ratio schedule related to control requirement.

a compromise between engine handling behavior and fuel consumption, the turbine pressure ratio is shown in Fig. 9. When it approaches to maximum low pressure spool speed, turbine pressure ratio is progressively reduced. For further pilot lever angle command, high pressure turbine temperature rises

considerably, high pressure spool speed rises slightly, and low pressure spool speed remains almost constant. During this process, in order to prevent the over-speed and over-temperature, the traditional control system makes the aircraft engine's acceleration a slow transition.

In accelerating control loop, it allows for independent setting of spool speed and turbine temperature, allowing engine working lines to be more closely "fitted" to surge line, with benefit to specific fuel consumption. The speed of response of a nozzle compared with the accelerating time of engine rotor permits rapid thrust control. But the surge margin is an important factor that will influence the accelerating progress, which is shown in Fig. 4.

In the aircraft engine control field, the control requirements of an engine may be classified into the following three aspects: (1) performance controls, for optimum engine operation; (2) limit controls for mechanical integrity; (3) change-of-state controls, mainly for engine handling.

Turbine temperature should not exceed a value determined by the properties of constructional materials. To accelerate an engine, fuel flow is increased; a too rapid increasing-rate of fuel flow may result in a breakdown of the airflow conditions within a compressor, causing engine surge. In order to satisfy the multi-objectives in aircraft engine control, the control system set up includes many sub-control loops, which is shown in Fig. 10. In Fig. 10, n_H is high pressure rotor speed; n_{Href} is reference of n_H; w_f is fuel flow; w_{fref} is reference of w_f and Ref is reference of limit parameter. But during the controller design process, there are many contradictions between the sub-control loops.

2.4. Problem of switching in aircraft engine control

The current application about switching in aircraft engine control is based on Min/Max switching law (see Fig. 11) and focuses mainly on the problem of stability, feedback stabilization. And this switching method is widely applied to engineering practice and is proved effective.

The typical feature of this class of switched control system is that it includes an integral saturating limit and a Min/Max switching law at the same time. The function of integral saturation limiting is to shorten switching delay time so that the system can be switched rapidly; the function of the Min/Max switching law is to select the control signals based on the minimum (maximum) value law. The coupled interactions between the integral saturation limiting and the Min/Max switching law result in that the two controllers are always competing to control the system hence the multi-objective control can be realized.

According to the above Fig. 11, for instance, the control signal u_2 in loop$_2$ is the minimum between the two loops,

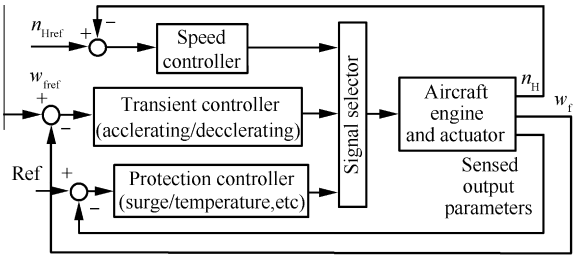

Fig. 10 Simplified diagram of the aircraft engine.

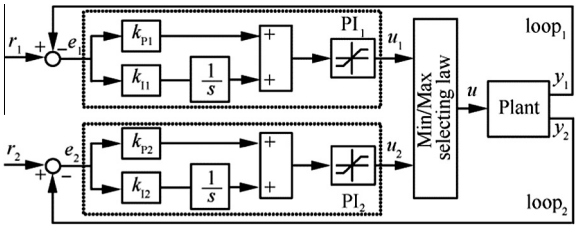

Fig. 11 A sketch map for multi-loop switched control system based on Min/Max switching law.

and loop$_1$ is inactive and will soon reach in a limit state finally due to an integral saturation limiting. When loop$_2$ is motivated under an outside input r_2, the output y_1 may exceed the setting limit r_1 in the control process of y_2, thus the PI$_1$ must be active to control y_1 in this case. The switching condition is that the control signal of loop$_1$ is equal to and less than that of loop$_2$.

If one controller is at work, the other one will be inactive. After the PI$_1$ has replaced the PI$_2$ to take over the system, the accumulated output at the initial stage has been high which may cause an dynamic overshoot of output y_1; moreover, as there is always a non-zero error input to PI$_2$, high output accumulated after a long integrating period will cause a change in the operation condition, which means it will cost more time to counteract this high output when the system need to be switched from loop$_1$ back to loop$_2$.

According to the shortage of Min/Max switching law, the paper proposes an example to show switching phenomena between the accelerating control loop (loop$_2$) and the temperature limitation control loop (loop$_1$) and the switching strategy is

$$\sigma_{plant}(t) = \begin{cases} 1, & T > T_{max} \\ 2, & T < T_{max} \end{cases} \tag{1}$$

and the simulation is shown in Fig. 12, Tables 1–3. In Fig. 12, n_L is low pressure rotor speed; T_4^* is turbine output temperature and Δw_f is variation of fuel flow. In Tables 1–3, H is altitude; Ma is Mach number; σ is overshoot and t_s is settle time.

We assume that the temperature limit is shown in Fig. 12(c). As accelerating sub-control loop fuel flow demand increases, T_4^* approaches the safe limit, and the temperature protection controller engages to control the engine. As expected, there are small glitches during controller switching and the tracking performance is acceptable.

However, this kind of switching method balances the performance and safety, somehow, sacrifices the system performance to guaranty the safety. It can be indicated that a key problem of how to increase switching rapidity to decrease the dynamic response overshoot in switching process should be focused for this class of multi-loop switched control system based on the switching law.

3. Smooth switching scheme design

3.1. Problem statement and preliminaries

Consider the switched control system

$$\begin{cases} \dot{\boldsymbol{x}}(t) = \boldsymbol{A}\boldsymbol{x}(t) + \boldsymbol{B}\boldsymbol{u}(t), \boldsymbol{x}(t_0) = \boldsymbol{x}(0) \\ \boldsymbol{u}(t) = \boldsymbol{u}_{\sigma(t)}(t) \\ \boldsymbol{y}(t) = \boldsymbol{C}\boldsymbol{x}(t) + \boldsymbol{D}\boldsymbol{u}(t) \end{cases} \tag{2}$$

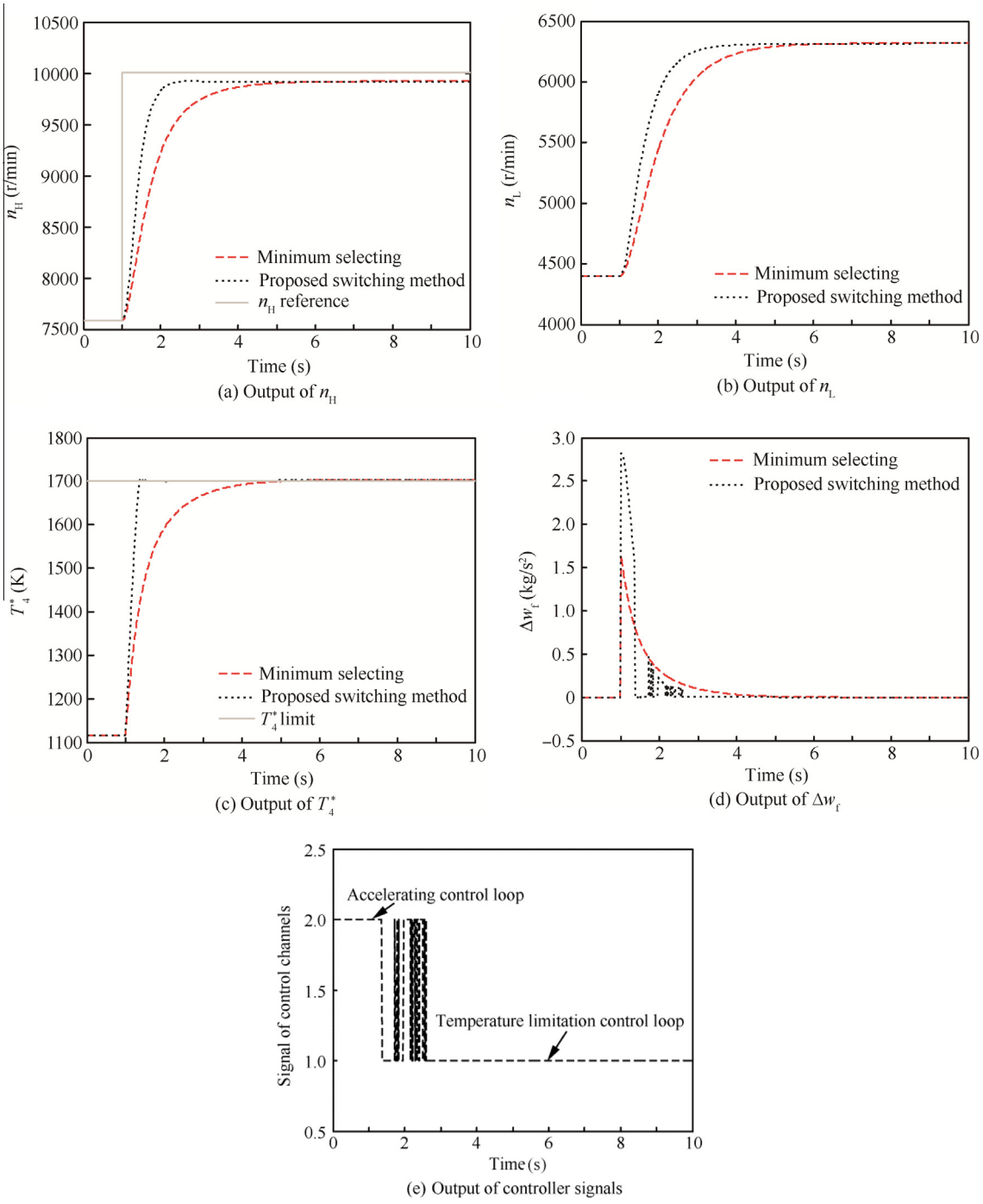

Fig. 12 Comparison of two different switching schemes.

where $\sigma(t)$:$[0, +\infty) \to P = \{1, 2, \cdots, N\}$ is the switching signal to be designed; $\boldsymbol{x}(t) \in \mathbf{R}^n$ is the system state, and $\boldsymbol{u}(t) \in \mathbf{R}^m$ the control input; $\boldsymbol{u}_{\sigma(t)}(t) \in \mathbf{R}^m$ represents the sub-controllers outputs and $\boldsymbol{y}(t) \in \mathbf{R}^l$ is the vector of system measurements; $\boldsymbol{A}$, $\boldsymbol{B}$, $\boldsymbol{C}$ and $\boldsymbol{D}$ are real constant matrices of appropriate dimensions. Corresponding to the switching signal $\sigma(t)$, we have the switching sequence

$$\Lambda = \{x_0; (i_0, t_0), (i_1, t_1), \cdots, (i_k, t_k), \cdots, |i_k \in P\}$$

When $t \in [t_k, t_{k+1}), \sigma(t) = i_k$, that is, the i_kth subsystem is activated.

A set of controllers can be designed in advanced based on the method in Ref.[23] as follows:

$$\kappa_i : \begin{cases} \dot{\boldsymbol{x}}_{\kappa_i}(t) = \boldsymbol{A}_{\kappa_i}\boldsymbol{x}_{\kappa_i}(t) + \boldsymbol{B}_{\kappa_i}\Delta\boldsymbol{y}_i \\ \boldsymbol{u}_i(t) = \boldsymbol{C}_{\kappa_i}\boldsymbol{x}_{\kappa_i}(t) + \boldsymbol{D}_{\kappa_i}\Delta\boldsymbol{y}_i \end{cases} \tag{3}$$

where $\boldsymbol{x}_{\kappa_i}(t) \in \mathbf{R}^{n_\kappa}$ is the ith controller state, and $\boldsymbol{A}_{\kappa_i}, \boldsymbol{B}_{\kappa_i}, \boldsymbol{C}_{\kappa_i}, \boldsymbol{D}_{\kappa_i}$ are the corresponding matrices; $\Delta\boldsymbol{y}_i$ is the

Table 1 Difference between two switching schemes ($H = 0$ km, $Ma = 0$).

Performance parameter	σ (%)		t_s (s)	
	Minimum selecting	Proposed switching method	Minimum selecting	Proposed switching method
n_H	0	0.048	1.24	0.61
n_L	0	0	1.90	1.14
T_4^*	0	0.117	1.20	0.29

Table 2 Difference between two switching schemes ($H = 5$ km, $Ma = 0.5$).

Performance parameter	σ (%)		t_s (s)	
	Minimum selecting	Proposed switching method	Minimum selecting	Proposed switching method
n_H	0	0.048	1.43	0.78
n_L	0	0	2.21	1.48
T_4^*	0	0.359	1.16	0.23

Table 3 Difference between two switching schemes ($H = 8$ km, $Ma = 0.6$).

Performance parameter	σ (%)		t_s (s)	
	Minimum selecting	Proposed switching method	Minimum selecting	Proposed switching method
n_H	0	0.054	1.54	1.04
n_L	0	0	2.59	2.02
T_4^*	0	0.159	0.99	0.32

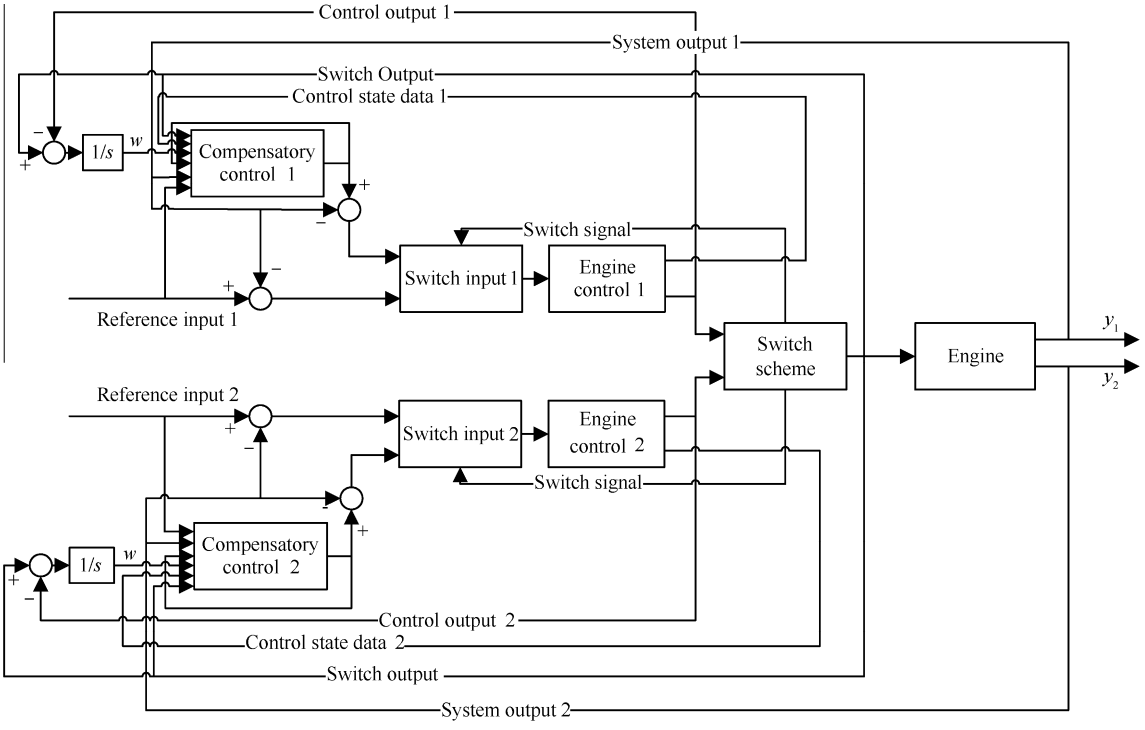

Fig. 13 Proposed smooth switching scheme.

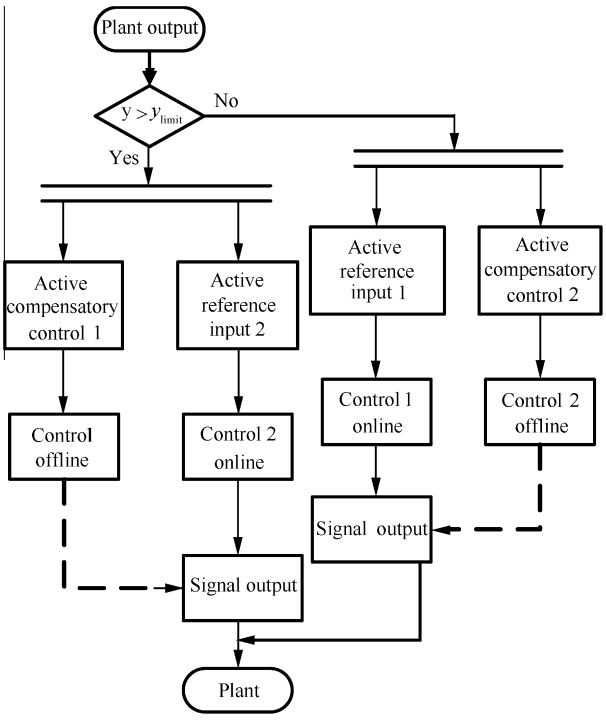

Fig. 14 Switching scheme process.

difference between the reference value $\boldsymbol{r}_i$ and the measured system output $\boldsymbol{y}_i$ ($\Delta \boldsymbol{y}_i = \boldsymbol{r}_i - \boldsymbol{y}_i$).

From the above simulation (shown in Fig. 12), we can find that the modified switching scheme can improve the aircraft engine performance; however, during switching, the switching signal has much oscillation. Therefore, the compensatory controller must be designed to deal this problem.

Integral action is used in classical control to eliminate steady state errors when tracking signals. It can be introduced into the linear quadratic (LQ) framework by considering the integral of the tracking error as an extra set of state variables. For any offline controller κ_i, $i \in P$, define the error state as

$$\dot{\boldsymbol{\omega}}_i = \boldsymbol{u}(t) - \boldsymbol{u}_i(t) = \boldsymbol{u}(t) - (\boldsymbol{C}_{\kappa_i}\boldsymbol{x}_{\kappa_i}(t) + \boldsymbol{D}_{\kappa_i}\Delta \boldsymbol{y}_i) \tag{4}$$

Definition 1[24]. Given a positive scalar $\varepsilon > 0$, a switching controller κ_i is said to perform a smooth switching if, whenever controller is switched, there exists a finite time $T_\varepsilon > 0$ such that the output of a controller κ_j to be switched satisfies the condition $\lim_{t \to T_\varepsilon} |\boldsymbol{u}(t) - \boldsymbol{u}_j(t)| \leqslant \varepsilon$, where $\boldsymbol{u}(t) = \boldsymbol{u}_i(t)$. In particular, κ_i is said to perform a strictly smooth switching $\lim_{t \to \infty} |\boldsymbol{u}(t) - \boldsymbol{u}_j(t)| = 0$.

The offline controller's input is transformed from system reference input $\boldsymbol{r}_i$ into compensatory controller output $\boldsymbol{r}_{C\kappa_i}$, Therefore, combining Eqs. (3) and (4), we can get the augmented system for the ith offline controller

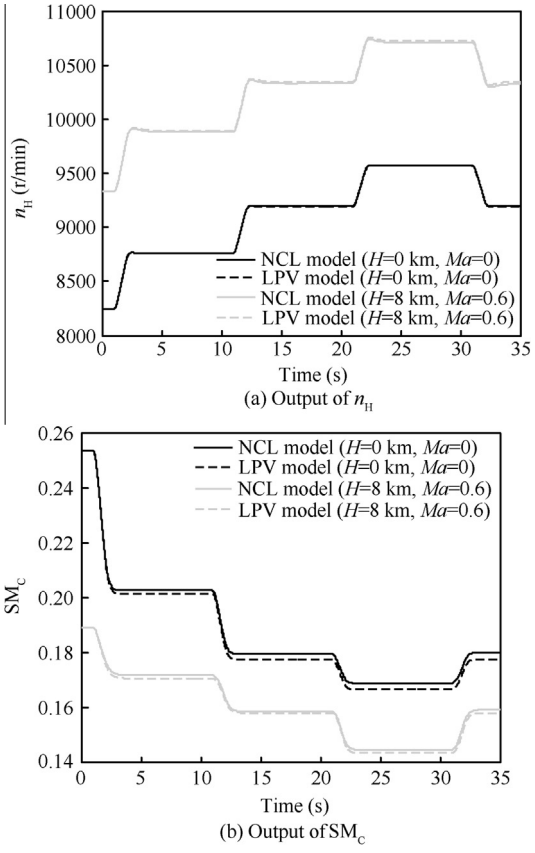

Fig. 15 Comparison of different models at different working points of whole flight envelope.

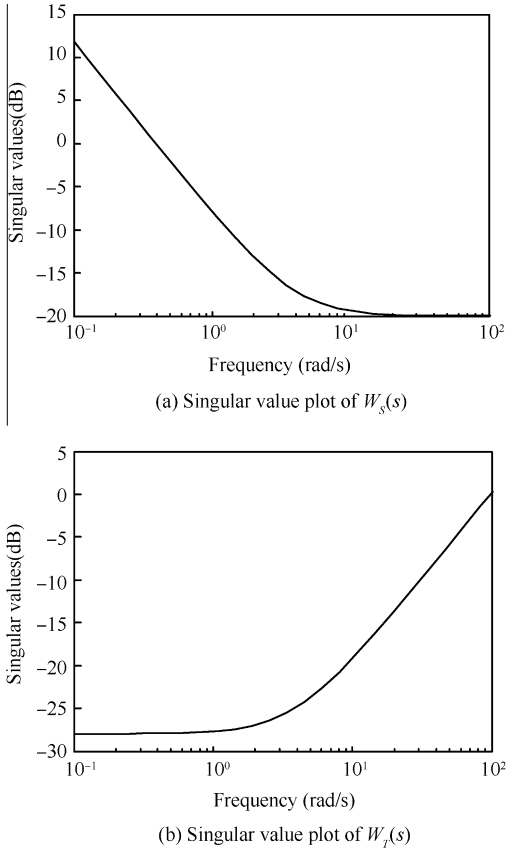

Fig. 16 Singular value in accelerating control loop.

$$\begin{bmatrix}\dot{\boldsymbol{x}}_{\kappa_i}(t)\\ \dot{\boldsymbol{\omega}}_i(t)\end{bmatrix}=\begin{bmatrix}\boldsymbol{A}_{\kappa_i} & \boldsymbol{0}\\ -\boldsymbol{C}_{\kappa_i} & \boldsymbol{0}\end{bmatrix}\begin{bmatrix}\boldsymbol{x}_{\kappa_i}(t)\\ \boldsymbol{\omega}_i(t)\end{bmatrix}+\begin{bmatrix}-\boldsymbol{B}_{\kappa_i}\\ \boldsymbol{D}_{\kappa_i}\end{bmatrix}\boldsymbol{y}_i(t)+\begin{bmatrix}\boldsymbol{B}_{\kappa_i}\\ -\boldsymbol{D}_{\kappa_i}\end{bmatrix}\boldsymbol{r}_{C\kappa_i}(t)+\begin{bmatrix}\boldsymbol{0}\\ \boldsymbol{I}\end{bmatrix}\boldsymbol{u}(t) \tag{5}$$

For simplicity, the augmented system (Eq. (5)) is rewritten as

$$\dot{\bar{\boldsymbol{x}}}_i(t)=\overline{\boldsymbol{A}}_i\bar{\boldsymbol{x}}_i(t)+\overline{\boldsymbol{B}}_{i_1}\boldsymbol{y}_i+\overline{\boldsymbol{B}}_{i_2}\boldsymbol{r}_{C\kappa_i}+\boldsymbol{M}\boldsymbol{u}(t) \tag{6}$$

where $\bar{\boldsymbol{x}}_i=\left[\boldsymbol{x}_{\kappa_i}^{\mathrm{T}},\boldsymbol{\omega}_i^{\mathrm{T}}\right]^{\mathrm{T}}$ is the augmented system state vector, $\overline{\boldsymbol{A}}_i=\begin{bmatrix}\boldsymbol{A}_{\kappa_i} & \boldsymbol{0}\\ -\boldsymbol{C}_{\kappa_i} & \boldsymbol{0}\end{bmatrix}$, $\overline{\boldsymbol{B}}_{i_1}=\begin{bmatrix}-\boldsymbol{B}_{\kappa_i}\\ \boldsymbol{D}_{\kappa_i}\end{bmatrix}$, $\overline{\boldsymbol{B}}_{i_2}=\begin{bmatrix}\boldsymbol{B}_{\kappa_i}\\ -\boldsymbol{D}_{\kappa_i}\end{bmatrix}$, $\boldsymbol{M}=\begin{bmatrix}\boldsymbol{0}\\ \boldsymbol{I}\end{bmatrix}$.

The compensatory controllers are designed by LQ method. The cost performance index for the design of the ith smooth switching compensatory controller is defined as

$$J_i=\frac{1}{2}\int_0^T\left(\bar{\boldsymbol{x}}_i^{\mathrm{T}}\boldsymbol{Q}_i\bar{\boldsymbol{x}}_i+\boldsymbol{v}_i^{\mathrm{T}}\boldsymbol{R}_i\boldsymbol{v}_i\right)\mathrm{d}t \tag{7}$$

where $\boldsymbol{Q}_i\geqslant\boldsymbol{0},\boldsymbol{R}_i>\boldsymbol{0}$ and $\boldsymbol{v}_i=\boldsymbol{r}_{C\kappa_i}-\boldsymbol{r}_i$ denote the difference between compensatory controller output $\boldsymbol{r}_{C\kappa_i}$ and system's reference signal $\boldsymbol{r}_i$. $\boldsymbol{Q}_i$ for state variables is standard in optimal control, while the $\boldsymbol{R}_i$ is used for scaling $\boldsymbol{v}_i$. The size of $\boldsymbol{v}_i$ will seriously influence the error size Eq. (4).

Therefore, when given a set of controllers (such as shown in Eq. (3)), a set of compensatory controllers is designed, respectively, such that the augmented system is stabilized and the number of switching times is minimized. And given a set of controllers and their compensatory controllers, a switching law $\sigma(t)$ is constructed and a sufficient condition is derived such that the closed-loop system composed of Eq. (3), Eq. (3) and compensatory controller is asymptotically stable and simultaneously guarantees the smooth switching by switching controllers.

3.2. Compensatory controller design

According to the above subsection's description, suppose that there exists a vector function $\boldsymbol{\lambda}_i(t)$, such that the quadratic form performance index function J_i can be rewritten as a non-conditional extremum problem

$$J_i=\frac{1}{2}\int_0^T\left(\boldsymbol{H}_i-\boldsymbol{\lambda}_i^{\mathrm{T}}\dot{\bar{\boldsymbol{x}}}_i\right)\mathrm{d}t \tag{8}$$

where the corresponding Hamiltonian function is

$$\begin{aligned}\boldsymbol{H}_i=&\left(\bar{\boldsymbol{x}}_i^{\mathrm{T}}\boldsymbol{Q}_i\bar{\boldsymbol{x}}_i+\boldsymbol{v}_i^{\mathrm{T}}\boldsymbol{R}_i\boldsymbol{v}_i\right)\\&+\boldsymbol{\lambda}_i^{\mathrm{T}}\left(\overline{\boldsymbol{A}}_i\bar{\boldsymbol{x}}_i+\overline{\boldsymbol{B}}_{i_1}\boldsymbol{y}_i+\overline{\boldsymbol{B}}_{i_2}\boldsymbol{r}_{C\kappa_i}+\boldsymbol{M}\boldsymbol{u}(t)\right)\end{aligned} \tag{9}$$

The necessary conditions of J_i are

$$\begin{cases}\dfrac{\partial\boldsymbol{H}_i}{\partial\boldsymbol{\lambda}_i}=\dot{\bar{\boldsymbol{x}}}_i\\ \dfrac{\partial\boldsymbol{H}_i}{\partial\bar{\boldsymbol{x}}_i}=-\dot{\boldsymbol{\lambda}}_i\\ \dfrac{\partial\boldsymbol{H}_i}{\partial\boldsymbol{r}_{C\kappa_i}}=\boldsymbol{0}\end{cases} \tag{10}$$

where

$$\frac{\partial\boldsymbol{H}_i}{\partial\bar{\boldsymbol{x}}_i}=\boldsymbol{Q}_i\bar{\boldsymbol{x}}_i+\overline{\boldsymbol{A}}_i^{\mathrm{T}}\boldsymbol{\lambda}_i=-\dot{\boldsymbol{\lambda}}_i \tag{11}$$

and

$$\frac{\partial\boldsymbol{H}_i}{\partial\boldsymbol{r}_{C\kappa_i}}=\boldsymbol{R}_i(\boldsymbol{r}_{C\kappa_i}-\boldsymbol{r}_i)+\overline{\boldsymbol{B}}_{i_2}^{\mathrm{T}}\boldsymbol{\lambda}_i=\boldsymbol{0} \tag{12}$$

and

$$\boldsymbol{r}_{C\kappa_i}=\boldsymbol{r}_i-\boldsymbol{R}_i^{-1}\overline{\boldsymbol{B}}_{i_2}^{\mathrm{T}}\boldsymbol{\lambda}_i \tag{13}$$

Taking Eq. (13) into Eq. (6), the compensatory controller's state space description is

$$\dot{\bar{\boldsymbol{x}}}_i=\overline{\boldsymbol{A}}_i\bar{\boldsymbol{x}}_i+\overline{\boldsymbol{B}}_{i_1}\boldsymbol{y}_i+\overline{\boldsymbol{B}}_{i_2}\left(\boldsymbol{r}_i-\boldsymbol{R}_i^{-1}\overline{\boldsymbol{B}}_{i_2}^{\mathrm{T}}\boldsymbol{\lambda}_i\right)+\boldsymbol{M}\boldsymbol{u}(t) \tag{14}$$

Suppose[25]

$$\boldsymbol{\lambda}_i(t)=\boldsymbol{P}_i(t)\bar{\boldsymbol{x}}_i(t)-\boldsymbol{g}_i(t) \tag{15}$$

and

$$\dot{\boldsymbol{\lambda}}_i(t)=\dot{\boldsymbol{P}}_i(t)\bar{\boldsymbol{x}}_i(t)+\boldsymbol{P}_i(t)\dot{\bar{\boldsymbol{x}}}_i(t)-\dot{\boldsymbol{g}}_i(t) \tag{16}$$

According to Eq. (11)

$$\begin{aligned}\dot{\boldsymbol{\lambda}}_i(t)&=-\boldsymbol{Q}_i\bar{\boldsymbol{x}}_i(t)-\overline{\boldsymbol{A}}_i^{\mathrm{T}}(\boldsymbol{P}_i(t)\bar{\boldsymbol{x}}_i(t)-\boldsymbol{g}_i(t))\\&=\overline{\boldsymbol{A}}_i^{\mathrm{T}}\boldsymbol{g}_i(t)-(\boldsymbol{Q}_i(t)+\overline{\boldsymbol{A}}_i^{\mathrm{T}}\boldsymbol{P}(t)_i)\bar{\boldsymbol{x}}_i(t)\end{aligned} \tag{17}$$

Taking Eqs. (14) and (15) into Eq. (16), we have

$$\begin{aligned}\dot{\boldsymbol{\lambda}}_i(t)=&\dot{\boldsymbol{P}}_i(t)\bar{\boldsymbol{x}}_i+\boldsymbol{P}_i(t)(\overline{\boldsymbol{A}}_i\bar{\boldsymbol{x}}_i+\overline{\boldsymbol{B}}_{i_1}\boldsymbol{y}_i+\overline{\boldsymbol{B}}_{i_2}\boldsymbol{r}_i)\\&-\boldsymbol{P}_i(t)\overline{\boldsymbol{B}}_{i_2}\boldsymbol{R}^{-1}\overline{\boldsymbol{B}}_{i_2}^{\mathrm{T}}(\boldsymbol{P}_i(t)\bar{\boldsymbol{x}}_i-\boldsymbol{g}_i(t))+\boldsymbol{P}_i(t)\boldsymbol{M}\boldsymbol{u}-\dot{\boldsymbol{g}}_i(t)\end{aligned} \tag{18}$$

Combining Eqs. (17) and (18) yields

$$\begin{aligned}&\left(\dot{\boldsymbol{P}}_i+\boldsymbol{P}_i\overline{\boldsymbol{A}}_i+\overline{\boldsymbol{A}}_i^{\mathrm{T}}\boldsymbol{P}_i-\boldsymbol{P}_i\overline{\boldsymbol{B}}_{i_2}\boldsymbol{R}_i^{-1}\overline{\boldsymbol{B}}_{i_2}^{\mathrm{T}}\boldsymbol{P}_i+\boldsymbol{Q}_i\right)\bar{\boldsymbol{x}}_i=\dot{\boldsymbol{g}}_i\\&+\left(\overline{\boldsymbol{A}}_i^{\mathrm{T}}-\boldsymbol{P}_i\overline{\boldsymbol{B}}_{i_2}\boldsymbol{R}_i^{-1}\overline{\boldsymbol{B}}_{i_2}^{\mathrm{T}}\right)\boldsymbol{g}_i-\boldsymbol{P}\overline{\boldsymbol{B}}_{i_1}\boldsymbol{y}_i-\boldsymbol{P}_i\overline{\boldsymbol{B}}_{i_2}\boldsymbol{r}_i-\boldsymbol{P}_i\boldsymbol{M}\boldsymbol{u}\end{aligned} \tag{19}$$

Note that the left side of Eq. (19) is a product of a function of time and state variables $\bar{\boldsymbol{x}}_i(t)$, while the right side is only a function of time. It means that for arbitrary t and $\bar{\boldsymbol{x}}_i(t)$, the following two equations

$$\begin{cases}-\dot{\boldsymbol{P}}_i=\boldsymbol{P}_i\overline{\boldsymbol{A}}_i+\overline{\boldsymbol{A}}_i^{\mathrm{T}}\boldsymbol{P}_i-\boldsymbol{P}_i\overline{\boldsymbol{B}}_{i_2}\boldsymbol{R}_i^{-1}\overline{\boldsymbol{B}}_{i_2}^{\mathrm{T}}\boldsymbol{P}_i+\boldsymbol{Q}_i\\ -\dot{\boldsymbol{g}}_i=(\overline{\boldsymbol{A}}_i^{\mathrm{T}}-\boldsymbol{P}_i\overline{\boldsymbol{B}}_{i_2}\boldsymbol{R}_i^{-1}\overline{\boldsymbol{B}}_{i_2}^{\mathrm{T}})\boldsymbol{g}_i-\boldsymbol{P}_i\overline{\boldsymbol{B}}_{i_1}\boldsymbol{y}_i\\ \qquad -\boldsymbol{P}_i\overline{\boldsymbol{B}}_{i_2}\boldsymbol{r}_i-\boldsymbol{P}_i\boldsymbol{M}\boldsymbol{u}\end{cases} \tag{20}$$

must be satisfied. When $t\to\infty$, $\dot{\boldsymbol{P}}_i(t)\to\boldsymbol{0}$ and $\dot{\boldsymbol{g}}_i(t)\to\boldsymbol{0}$, Eq. (20) can be rewritten as

$$\begin{cases}\boldsymbol{0}=\boldsymbol{P}_i\overline{\boldsymbol{A}}_i+\overline{\boldsymbol{A}}_i^{\mathrm{T}}\boldsymbol{P}_i-\boldsymbol{P}_i\overline{\boldsymbol{B}}_{i_2}\boldsymbol{R}_i^{-1}\overline{\boldsymbol{B}}_{i_2}^{\mathrm{T}}\boldsymbol{P}_i+\boldsymbol{Q}_i\\ \boldsymbol{0}=(\overline{\boldsymbol{A}}_i^{\mathrm{T}}-\boldsymbol{P}_i\overline{\boldsymbol{B}}_{i_2}\boldsymbol{R}_i^{-1}\overline{\boldsymbol{B}}_{i_2}^{\mathrm{T}})g_i\\ \qquad -\boldsymbol{P}_i\overline{\boldsymbol{B}}_{i_1}\boldsymbol{y}_i-\boldsymbol{P}_i\overline{\boldsymbol{B}}_{i_2}\boldsymbol{r}_i-\boldsymbol{P}_i\boldsymbol{M}\boldsymbol{u}\end{cases} \tag{21}$$

and

$$\boldsymbol{g}_i=\left(\overline{\boldsymbol{A}}_i^{\mathrm{T}}-\boldsymbol{P}_i\overline{\boldsymbol{B}}_{i_2}\boldsymbol{R}_i^{-1}\overline{\boldsymbol{B}}_{i_2}^{\mathrm{T}}\right)^{-1}\left(\boldsymbol{P}_i\overline{\boldsymbol{B}}_{i_1}\boldsymbol{y}_i+P_i\overline{\boldsymbol{B}}_{i_2}\boldsymbol{r}_i+\boldsymbol{P}_i\boldsymbol{M}\boldsymbol{u}(t)\right) \tag{22}$$

where $\boldsymbol{P}_i$ is the solution of algebraic Riccati Eq. (21).

Thus, according to Eqs. (13), (15), (22), the compensatory controller output can be carried out

$$\bar{\boldsymbol{r}}_{C\kappa_i}=\boldsymbol{K}_{r_i}\boldsymbol{r}_i+\boldsymbol{K}_{x_{\kappa_i}}\boldsymbol{x}_{\kappa_i}+\boldsymbol{K}_{\omega_i}\boldsymbol{\omega}_i+\boldsymbol{K}_{y_i}\boldsymbol{y}_i+\boldsymbol{K}_{u_i}\boldsymbol{u} \tag{23}$$

where $\boldsymbol{K}_{r_i}=\boldsymbol{I}+\boldsymbol{R}_i^{-1}\overline{\boldsymbol{B}}_{i_2}^{\mathrm{T}}\left(\overline{\boldsymbol{A}}_i^{\mathrm{T}}-\boldsymbol{P}_i\overline{\boldsymbol{B}}_{i_2}\boldsymbol{R}_i^{-1}\overline{\boldsymbol{B}}_{i_2}^{\mathrm{T}}\right)^{-1}\boldsymbol{P}_i\overline{\boldsymbol{B}}_{i_2}$, $[\boldsymbol{K}_{x_{\kappa_i}}\quad\boldsymbol{K}_{\omega_i}]=-\boldsymbol{R}_i^{-1}\overline{\boldsymbol{B}}_{i_2}^{\mathrm{T}}\boldsymbol{P}_i,\boldsymbol{K}_{y_i}=\boldsymbol{R}_i^{-1}\overline{\boldsymbol{B}}_{i_1}^{\mathrm{T}}\left(\overline{\boldsymbol{A}}_i^{\mathrm{T}}-\boldsymbol{P}_i\overline{\boldsymbol{B}}_{i_2}\boldsymbol{R}_i^{-1}\overline{\boldsymbol{B}}_{i_2}^{\mathrm{T}}\right)^{-1}\boldsymbol{P}_i\overline{\boldsymbol{B}}_{i_1}$, $\boldsymbol{K}_{u_i}=\boldsymbol{R}_i^{-1}\overline{\boldsymbol{B}}_{i_2}^{\mathrm{T}}\left(\overline{\boldsymbol{A}}_i^{\mathrm{T}}-\boldsymbol{P}_i\overline{\boldsymbol{B}}_{i_2}\boldsymbol{R}_i^{-1}\overline{\boldsymbol{B}}_{i_2}^{\mathrm{T}}\right)^{-1}\boldsymbol{P}_i\boldsymbol{M}$

The design of compensatory controller's output is shown in Fig. 13. An off-line controller is closed by its compensatory controller to drive the control signal close to the online one. And the switching scheme process is shown in Fig. 14.

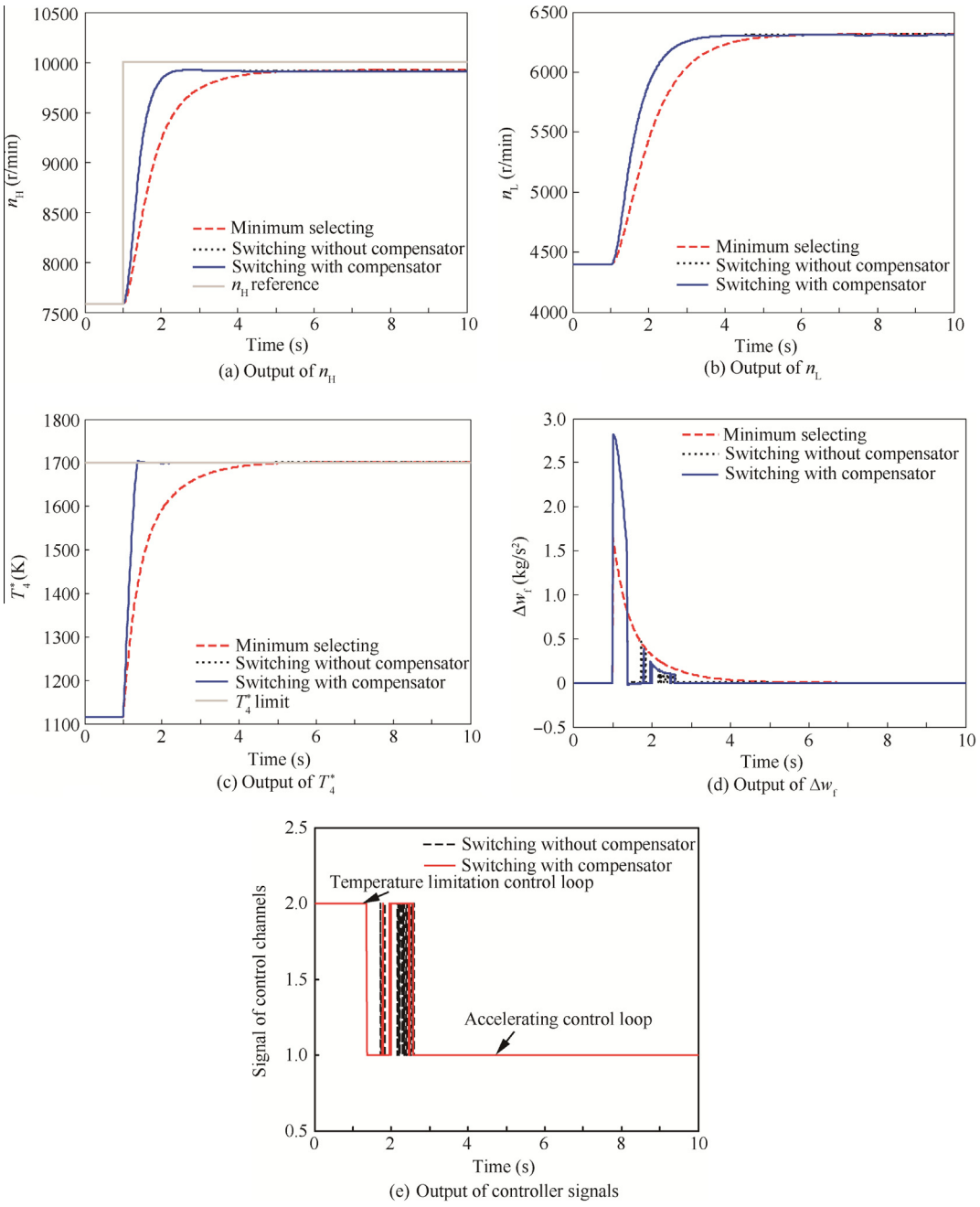

Fig. 17 Comparison of different switching schemes (accelerating switching with temperature limitation sub-control loops at $H = 0$ km, $Ma = 0$).

Table 4 Difference between two switching schemes (accelerating switching with temperature limitation sub-control loops at $H = 0$ km, $Ma = 0$).

Performance parameter	σ (%)			t_s (s)		
	Minimum selecting	Switching without compensator	Switching with compensator	Minimum selecting	Switching without compensator	Switching with compensator
n_H	0	0.048	0.134	1.24	0.61	0.60
n_L	0	0	0	1.90	1.14	1.13
T_4^*	0	0.117	0.241	1.20	0.29	0.28

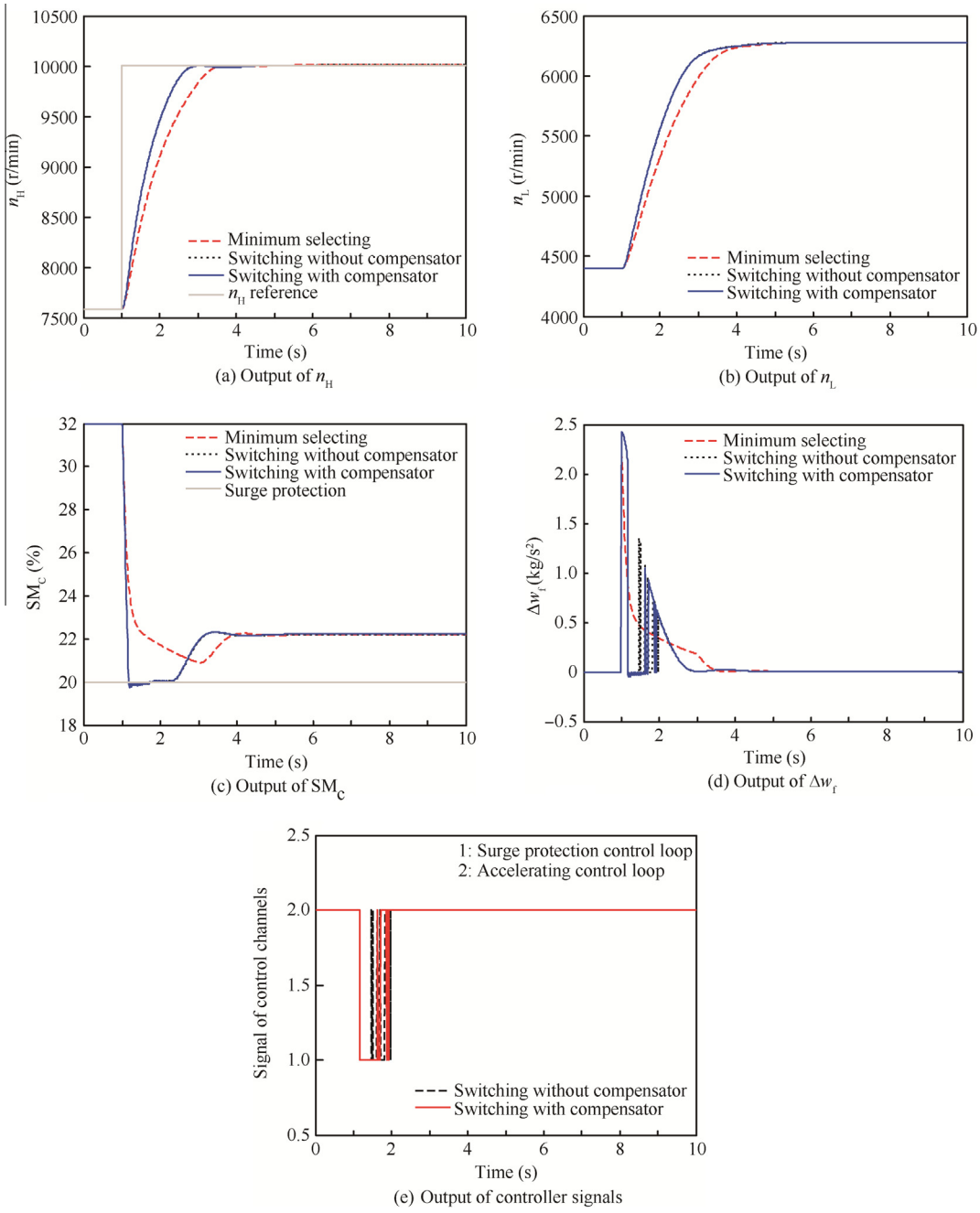

Fig. 18 Comparison of different switching schemes (accelerating switching with surge protection sub-control loops at $H = 0$ km, $Ma = 0$).

4. Control design procedure and simulation results

4.1. Augmented aircraft engine model

In order to analyze the time-domain performance objectives, the linear parameter-varying (LPV) model[26–28] of the form is drawn:

$$\begin{cases} \dot{\boldsymbol{x}}(t) = \boldsymbol{A}(\boldsymbol{\rho}(t))\boldsymbol{x}(t) + \boldsymbol{B}(\boldsymbol{\rho}(t))\boldsymbol{u}(t) \\ \boldsymbol{y}(t) = \boldsymbol{C}(\boldsymbol{\rho}(t))\boldsymbol{x}(t) + \boldsymbol{D}(\boldsymbol{\rho}(t))\boldsymbol{u}(t) \end{cases} \tag{24}$$

where $\boldsymbol{x}(t) = [n_H, n_L]^T$, $u(t) = w_f$, the scheduling parameter is selected as $\rho(t) = n_H$, and $y(t)$ denotes the aircraft engine measured outputs, such as n_H, n_L, p_3, T_4^*, and performance parameters' outputs, such as F (thrust), SM_C (surge margin of compressor), and so on. The following simulations show the comparison of LPV model and NCL model.

The results obtained from simulation of the engine n_H and SM_C LPV model are compared with NCL model results in Fig. 15(a). The n_H increases with an increase in w_f. The model output precision is $\pm 1.5\%$. Throughout the analysis of the operating points, when given the flight condition (such as $H = 8$ km and $Ma = 0.6$), the increasing spool speed results in decreasing magnifying coefficient and time coefficient. Furthermore, the dynamic response becomes faster. The comparison of SM_C is shown in Fig. 15(b).

4.2. Smooth switching controller tuning procedure

Firstly, according to the Section 3.1, the form of accelerating controller, temperature limit controller and surge protection controller is respectively.

$$\kappa_{\mathrm{ACC}}:\begin{cases}\dot{\boldsymbol{x}}_{\mathrm{ACC}}=\boldsymbol{A}_{\mathrm{ACC}}\boldsymbol{x}_{\mathrm{ACC}}+\boldsymbol{B}_{\mathrm{ACC}}(r_{\mathrm{ACC}}-n_{\mathrm{Hmes}})\\ u_{\mathrm{ACC}}=\boldsymbol{C}_{\mathrm{ACC}}\boldsymbol{x}_{\mathrm{ACC}}+\boldsymbol{D}_{\mathrm{ACC}}(r_{\mathrm{ACC}}-n_{\mathrm{Hmes}})\end{cases} \tag{25}$$

$$\kappa_{\mathrm{T}}:\begin{cases}\dot{\boldsymbol{x}}_{\mathrm{T}}=\boldsymbol{A}_{\mathrm{T}}\boldsymbol{x}_{\mathrm{T}}+\boldsymbol{B}_{\mathrm{T}}(r_{\mathrm{T}}-T^{*}_{4\ \mathrm{mes}})\\ u_{\mathrm{T}}=\boldsymbol{C}_{\mathrm{T}}\boldsymbol{x}_{\mathrm{T}}+\boldsymbol{D}_{\mathrm{T}}(r_{\mathrm{T}}-T^{*}_{4\ \mathrm{mes}})\end{cases} \tag{26}$$

$$\kappa_{\mathrm{SMC}}:\begin{cases}\dot{\boldsymbol{x}}_{\mathrm{SMC}}=\boldsymbol{A}_{\mathrm{SMC}}\boldsymbol{x}_{\mathrm{SMC}}+\boldsymbol{B}_{\mathrm{SMC}}(r_{\mathrm{SMC}}-\mathrm{SM}_{\mathrm{Cmes}})\\ u_{\mathrm{SMC}}=\boldsymbol{C}_{\mathrm{SMC}}\boldsymbol{x}_{\mathrm{SMC}}+\boldsymbol{D}_{\mathrm{SMC}}(r_{\mathrm{SMC}}-\mathrm{SM}_{\mathrm{Cmes}})\end{cases} \tag{27}$$

where the subscripts of Eqs. (25)–(27) are: "ACC" is accelerating control loop, "T" represents temperature limit control loop, "SMC" is surge margin control loop and "mes" means measured parameter.

The controllers are designed to achieve the following robustness and performance specifications. In the accelerating sub-control loop, the controller is tuned such that steady-state tracking error is zero. The settling time is expected to be within 1.5 s.

In this paper, the mixed sensitivity synthesis design method is used to deal with the three sub-controllers. The sensitivity weighting function $W_S(s)$ is chosen to be large at low frequency in order to obtain good command tracking at low frequency. The complementary sensitivity weighting function $W_T(s)$ is chosen to be large at high frequency to obtain robustness to unmodeled high frequency dynamics. The sensitivity and complimentary sensitivity weighting functions are designed as two parallel first-order lags and leads, respectively, with the low frequency magnitudes and crossover frequencies specified by the user.

Here $W_S(s)$ should have the characteristic of low-pass frequency, and the unity-gain crossover frequencies of 0.4 rad/s. In order to satisfy the bandwidth requirement, $W_T(s)$'s static gain should be adequately small, and it should exhibit a unity-gain crossover frequencies of 100 rad/s. According to the above specifications, the weighting functions are chosen as follows (see Fig. 16).

In the protection/limit sub-control loops, the weighting functions are the same as the accelerating sub-control loop, and the controllers of each control loop are

$$\begin{cases}\kappa_{\mathrm{ACC}}=\dfrac{0.001s+10^{-6}}{s}\\ \kappa_{T}=\dfrac{0.005s+10^{-5}}{s}\\ \kappa_{\mathrm{SMC}}=\dfrac{-20s+10^{-5}}{s}\end{cases} \tag{28}$$

4.3. Simulation results

In this section, we use the controllers which are optimized above to the aircraft engine LPV model. The following parameters of accelerating sub-control compensator were designed at $H = 0$ km, $Ma = 0$ operating point and the same condition with temperature limit and surge protection compensators.

$$\overline{\boldsymbol{A}}_{\mathrm{ACC}}=\begin{bmatrix}0 & 0\\ 10^{-6} & 0\end{bmatrix},\ \overline{\boldsymbol{B}}_{\mathrm{ACC}_1}=\begin{bmatrix}-1\\ 0.001\end{bmatrix},$$

$$\overline{\boldsymbol{B}}_{\mathrm{ACC}_2}=\begin{bmatrix}1\\ -0.001\end{bmatrix},\quad \boldsymbol{M}=\begin{bmatrix}0\\ 1\end{bmatrix},$$

$$\boldsymbol{Q}=\begin{bmatrix}11 & 0\\ 0 & 11\end{bmatrix},\quad \boldsymbol{R}=1,$$

$$\boldsymbol{P}_{\mathrm{ACC}}=\begin{bmatrix}14.2990301346208 & 10985.7193189240\\ 10985.7193189236 & 10989035.9518960\end{bmatrix},$$

$$K_{r_{\mathrm{ACC}}}=-10.0000143166330,$$

$$K_{\boldsymbol{x}_{\kappa_{\mathrm{ACC}}}}=-3.31331081569725,$$

$$K_{\omega_{\mathrm{ACC}}}=3.31663297194973,$$

$$K_{y_{\mathrm{ACC}}}=11.0000143166333,$$

$$K_{u_{\mathrm{ACC}}}=0.011000000029860.$$

$$\overline{\boldsymbol{A}}_{\mathrm{T}}=\begin{bmatrix}0 & 0\\ 10^{-5} & 0\end{bmatrix},\quad \overline{\boldsymbol{B}}_{\mathrm{T}_1}=\begin{bmatrix}-1\\ 0.005\end{bmatrix},$$

$$\overline{\boldsymbol{B}}_{\mathrm{T}_2}=\begin{bmatrix}1\\ -0.005\end{bmatrix},\quad \boldsymbol{M}=\begin{bmatrix}0\\ 1\end{bmatrix},$$

$$\boldsymbol{Q}=\begin{bmatrix}11 & 0\\ 0 & 11\end{bmatrix},\quad \boldsymbol{R}=1,$$

$$\boldsymbol{P}_{\mathrm{T}}=\begin{bmatrix}30.6464335407947 & 5469.26808301907\\ 5469.26808301941 & 1094516.94148650\end{bmatrix},$$

$$K_{r_{\mathrm{T}}}=-10.0003081662441,$$

$$K_{\boldsymbol{x}_{\kappa_{\mathrm{T}}}}=-3.30009312569769,$$

$$K_{\omega_{\mathrm{T}}}=3.31662441345543,$$

$$K_{y_{\mathrm{T}}}=11.0003081662441,$$

$$K_{u_{\mathrm{T}}}=0.0549999999977263.$$

Simulation 1: Switching process between accelerating and temperature sub-loops. In order to show the switching between the two sub-controllers in a harsh condition, the reference input of the accelerating speed is given in Fig. 17(a).

Assume that the temperature limit is as shown in Fig. 17(c). As accelerating sub-control loop speed demand increases, the

Table 5 Difference between two switching schemes (accelerating switching with surge protection sub-control loops at $H = 0$ km, $Ma = 0$).

Performance parameter	σ (%)			t_s (s)		
	Minimum selecting	Switching without compensator	Switching with compensator	Minimum selecting	Switching without compensator	Switching with compensator
n_{H}	0	0	0	1.47	1.05	1.05
n_{L}	0	0	0	1.96	1.51	1.51
$\mathrm{SM_C}$	5.878	10.8	0.241	2.19	1.73	1.71

temperature approaches the safe limit, and the temperature limit controller is in charge of controlling the engine. As expected, there are small glitches during controller switching, and the tracking performance is acceptable. The difference of performance between two switching schemes is shown in Table 4.

Simulation 2: Switching process between accelerating and surge protection two sub-loops.

$$\overline{\boldsymbol{A}}_{\mathrm{SMC}} = \begin{bmatrix} 0 & 0 \\ 10^{-5} & 0 \end{bmatrix}, \quad \overline{\boldsymbol{B}}_{\mathrm{SMC}_1} = \begin{bmatrix} -1 \\ -20 \end{bmatrix},$$

$$\overline{\boldsymbol{B}}_{\mathrm{SMC}_2} = \begin{bmatrix} 1 \\ 20 \end{bmatrix}, \quad \boldsymbol{M} = \begin{bmatrix} 0 \\ 1 \end{bmatrix},$$

$$\boldsymbol{Q} = \begin{bmatrix} 0.05 & 0 \\ 0 & 0.05 \end{bmatrix}, \quad \boldsymbol{R} = 1,$$

$$\boldsymbol{P}_{\mathrm{SMC}} = \begin{bmatrix} 79419491.887 & -3970974.150 \\ -3970974.150 & 198548.696 \end{bmatrix},$$

$$K_{r_{\mathrm{SMC}}} = -19.0500022005290,$$

$$K_{x_{r_{\mathrm{SMC}}}} = -8.87945564091206,$$

$$K_{\omega_{\mathrm{SMC}}} = 0.220086625311524,$$

$$K_{y_{\mathrm{SMC}}} = 20.0500022005290,$$

$$K_{u_{\mathrm{SMC}}} = -0.999999993946403.$$

The simulation results are shown in Fig. 18. We can obtain the detailed characterization as shown in Table 5, the smooth switching performance indices of overshoot and settling time of $\mathrm{SM_C}$ obtained by Min selecting law and switching without compensator are 5.878%, 10.8%, and 2.19 s, 1.73 s, respectively. However, the indices obtained by switching method with compensator are much smaller, which are 0.241% and 1.71 s, respectively. Thus, it clearly demonstrates that the proposed method achieves a better smooth switching performance.

5. Conclusions

In this paper, the aircraft engine multi-loop control system is described in detail and the switching control theory is introduced to solve the regulating and protecting control problems. This paper might give a positive thought that the switching performance objectives and the switching scheme are given and a family of PID controllers and compensators is designed.

Firstly, a new switching scheme has been proposed, throughout the comparison with traditional switching method (Min/Max switching law), the performance indices can be improved better. However, the frequency switching cannot be avoided. After that, a smooth switching method has been investigated based on the optimal theory and the internal model principle. Finally, two examples have confirmed the effectiveness of the proposed bumpless switching approach. The simulations show that using the method can not only improve the dynamic performance of the engine control system, but also can guarantee the stability in some occasions. In that way, the conservatism is reduced, the dynamic performance is improved and the multi-loop controllers are regulated well.

Acknowledgments

The authors are grateful to Prof. Ming Cao and Dr. Tao Liu from University of Groningen for discussions. They would also like to thank the anonymous reviewers for their critical and constructive review of the manuscript. This study was supported by the National Natural Science Foundation of China (Grant No. 61104146/F030203) and Innovation Plan of Aero Engine Complex System Safety by the Ministry of Education Chang Jiang Scholars of China (Grant No. IRT0905).

References

1. Skira CA, Agnello M. Control systems for the next century's fighter engines. *J Eng Gas Turbines Power* 1992;**114**(4):749–54.
2. Jaw LC, Mattingly JD. *Aircraft engine controls: design, system analysis and health monitoring*. Reston: AIAA; 2009.
3. Blakelock JH. Automatic control of aircraft and missiles. New York: Wiley; 1991.
4. Garg S. Robust integrated flight/propulsion control design for a STOVL aircraft using H_∞ control design techniques. *Automatica* 1993;**29**(1):129–45.
5. Liu XF, Zhao L. Approximate nonlinear modeling of aircraft engine surge margin based on equilibrium manifold expansion. *Chin J Aeronaut* 2012;**25**(5):663–74.
6. Isidori A. *Nonlinear control systems*. New York: Springer-Verlag; 1999.
7. Littleboy DM, Smith PR. Using bifurcation methods to aid nonlinear dynamic inversion control law design. *J Guid Control Dyn* 1998;**21**(4):632–8.
8. Snell SA, Nns DF, Arrard WL. Nonlinear inversion flight control for a supermaneuverable aircraft. *J Guid Control Dyn* 1992;**15**(4):976–84.
9. Mulgund SS, Stengel RF. Aircraft flight control in wind shear using sequential dynamic inversion. *J Guid Control Dyn* 1995;**18**(5):1084–91.
10. Samar R, Postlethwaite I. Multivariable controller design for a high performance aero-engine. *Proceedings of international conference on control*, Vol. 94; 1994. p. 1312–7.
11. Frederick DK, Garg S, Adibhatla S. Turbofan engine control design using robust multivariable control technologies. *IEEE Trans Control Syst Technol* 2000;**8**(6):961–70.
12. Peleties P, Decarlo R. Asymptotic stability of *m*-switched systems using Lyapunov-like functions. *Proceedings of American control conference*; 1991 Jun 26–28; Boston, MA; 1991. p. 1679–84.
13. Branicky MS. Multiple Lyapunov functions and other analysis tools for switched and hybrid systems. *IEEE Trans Autom Control* 1998;**43**(4):475–82.
14. Pettersson S, Lennartson B. Stability and robustness for hybrid systems. *Proceedings of the 35th IEEE conference on decision and control*; 1996 Dec 11–13; Kobe. 1996. p. 1202–7.
15. Ye H, Michel AN, Hou L. Stability theory for hybrid dynamical systems. *IEEE Trans Autom Control* 1998;**43**(4):461–74.
16. Daafouz J, Riedinger P, Iung C. Stability analysis and control synthesis for switched systems: a switched Lyapunov function approach. *IEEE Trans Autom Control* 2002;**47**(11):1883–7.
17. Hu B, Zhai G, Michel A. Hybrid static output feedback stabilization of second-order linear time-invariant systems. *Linear Algebra Appl* 2002;**351**:475–85.
18. Liberzon D. Stabilizing a linear system with finite-state hybrid output feedback. *Proceedings of the 7th IEEE mediterranean conference on control and automation*; 1999.
19. Litsyn E, Nepomnyashchikh YV, Ponosov A. Stabilization of linear differential systems via hybrid feedback controls. *SIAM J Control Optim* 2000;**38**(5):1468–80.
20. Artstein Z. *Examples of stabilization with hybrid feedback. Hybrid systems III*. Heidelberg: Springer; 1996. p. 173–85.
21. Zhai G, Chen X. Stabilizing linear time-invariant systems with finite-state hybrid static output feedback. *Proceedings of IEEE international symposium on circuits and systems*; 2002. p. 249–52.

22. Savkin AV, Evans RJ. Robust output feedback stabilizability via controller switching. *Proceedings of the 35th IEEE conference on decision and control*; 1996 Dec 11–13; Kobe. 1996. p. 2654–8.
23. Mu J, Rees D, Liu GP. Advanced controller design for aircraft gas turbine engines. *Control Eng Pract* 2005;**13**(8):1001–15.
24. Bao W, Qi Y, Yu D, Yao Z, Zhao J. Bumpless switching scheme design and its application to hypersonic vehicle model. *Int J Innov Comput Inf Control* 2012;**8**(1):677–89.
25. Sternad M, Ahlén A. LQ controller design and self-tuning control. *IEE Control Eng Ser* 1993;56.
26. Bruzelius F. *Linear parameter-varying systems dissertation*. Göteborg, Sweden: Chalmers University of Technology; 2004.
27. Balas GJ. Linear, parameter-varying control and its application to a turbofan engine. *Int J Robust Nonlinear Control* 2002;**12**(9):763–96.
28. Bamieh B, Giarre L. Identification of linear parameter varying models. *Int J Robust Nonlinear Control* 2002;**12**(9):841–53.

Liu Xiaofeng is a teacher and postgraduate supervisor at School of Transportation Science and Engineering, Beihang University. He received the B.S., M.S. and Ph.D. degrees in power machinery engineering from Harbin Institute of Technology in 2002, 2004 and 2008, respectively. His main research interests are dynamic modeling and control of aircraft engine.

Shi Jing is a postgraduate student at School of Transportation Science and Engineering, Beihang University. He received his B.S. degree from Beihang University in 2012. His area of research includes dynamic modeling and control of aircraft engine.

Qi Yiwen is a teacher at School of Automation, Shenyang Aerospace University. He received B.S. degree and M.S. degree in applied mathematics from Harbin Normal University in 2005 and Heilongjiang University in 2008, respectively, and the Ph.D. degree in power machinery and engineering from Harbin Institute of Technology in 2012. His research interests include switching control, robust control, and their applications in flight vehicle and aeroengine.

Yuan Ye is Ph.D. candidate student at School of Energy and Power Engineering, Beihang University. He received his B.S. degree from Civil Aviation University of China, and M.S. degree from Beihang University in power machinery. His area of research includes modeling and control of aircraft engine.